R-823

EVALUATION OF THERMAL BARRIER COATINGS FROM BURNER RIG TESTS

J-P. Immarigeon, V.R. Parameswaran, D. Chow and D.D. Morphy
Institute for Aerospace Research
National Research Council of Canada
Ottawa, Ontario, K1A 0R6

P. Gougeon, M. Prystay and C. Moreau
Industrial Materials Institute
National Research Council of Canada
Boucherville, Quebec, J4B 6Y4

SUMMARY

A series of thermal barrier coatings were deposited on superalloy pins by various techniques using different processing parameters, in order to optimize the durability of the coatings for aerospace applications. These coatings were subjected to simulated high temperature engine operating conditions in a high velocity burner rig. The durability of the coatings at different temperatures was assessed at regular intervals from changes in pin weight due to oxidation and/or loss of coating. The thermal characteristics of some of the coatings were also assessed on-line by monitoring the core temperatures of the pins. After thermal cycling, the specimens were subjected to metallographic examination, to study the change in microstructure brought about by the burner rig cyclic tests. The test methodology and the results are discussed.

1. INTRODUCTION

Thermal barrier coatings (TBC's), as the name implies, are protective barriers used to isolate turbine components (usually cooled by air flow from the compressor) from the high temperature of the engine, so that the temperature felt by the substrate is considerably lower than that in which the component is operating. Lowering the metal temperature improves the creep life and reduces the thermal stresses induced by transients caused by accelerations and decelerations in the engine. Thermal barrier coatings consist of a metallic bond coat, usually MCrAlY (where M stands for Ni, Co, Fe, or a combination of these) of thickness up to 150 μm, over which a ceramic oxide overlay coating of thickness up to 500 μm is applied. The bond coat layer has higher oxidation and hot corrosion resistance than the superalloy substrate material and it also provides a base for mechanical bonding of the ceramic layer to the metal.

The most widely used ceramic overlay coating is based on zirconia, which has a thermal expansion coefficient close to that of the superalloy substrate. Pure zirconia, however, undergoes phase transformation in the temperature range of gas turbine engine operation. Above 2370°C, ZrO_2 exists in the cubic form and as it cools down below 2370°C, it transforms to the tetragonal form, which in turn undergoes solid state transformation to the monoclinic phase below 1170°C. This latter phase change (tetragonal to monoclinic) is accompanied by a volume increase of about 9%, which will cause cracking and lead to spalling of the ceramic zirconia layer from the bond coat. This phase transformation, however, can be suppressed by the addition of stabilizing agents such as Y_2O_3, MgO, CeO_2 and CaO, which lower the phase transformation temperature. Of these, yttria has been found to be a good stabilizer for the range of turbine operating temperatures and partially stabilized zirconia containing 8%Y_2O_3 (called YPSZ), has been found to perform well in aero engines (**1**). Other ceramic systems based on various oxides (e.g. MgO, CeO, and CaO) and oxide mixtures as well as metal silicates (e.g. Ca_2SiO_4, $ZrSiO_4$) have also been considered for marine applications where hot corrosion is a concern (**2**).

TBC's can be applied by one of several methods, including flame spraying, plasma spraying, detonation gun projection, and electron beam physical vapour deposition (EBPVD). Several modifications and innovations have been made in these techniques to suit particular applications and to obtain coatings of high integrity and durability (**3-5**). Plasma spraying, for example, has been carried out under low pressure (partial vacuum) to produce coatings of higher density. In a recent NASA Tech Brief (October 1996, p 97), it has been reported that a vacuum plasma sprayed zirconia TBC endured five times as many engine stop/start cycles as coatings applied in air (**6**). Using EBPVD, graded coatings with gradual transition of composition and properties through the thickness have been produced. This will prevent an abrupt transition zone, where the likelihood of failure can be high due to drastic differences in the properties of the metallic and ceramic layers (**7**). Nano-structured TBC's (containing nanograins or nanolayers) could provide the basis for new generations of TBC's (**8**).

The microstructures of TBC's vary significantly with deposition technique. Typical microstructures of coatings applied by air plasma spraying (APS), vacuum plasma

Paper presented at an AGARD SMP Meeting on "Thermal Barrier Coatings", held in Aalborg, Denmark, 15-16 October 1997, and published in R-823.

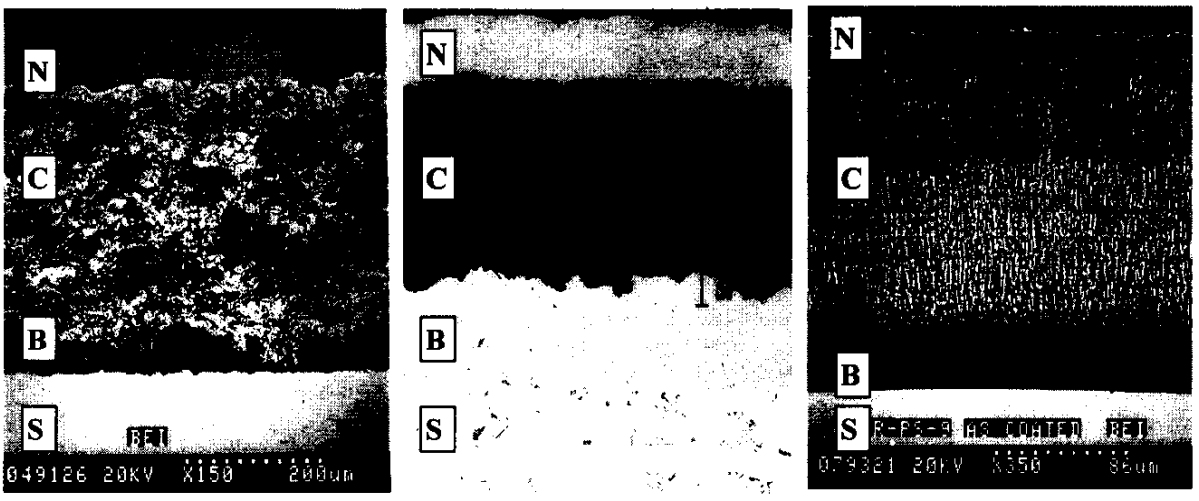

Figure 1 Representative microstructures of TBC's applied by (a) plasma spraying in air (b) vacuum plasma spraying and (c) EBPVD (S: substrate, B: bond coat, C: ceramic overlay layer, N: electroless Ni film used to protect ceramic for metallography).

spraying (VPS) and electron beam physical vapour deposition (EBPVD) are shown in **Figure 1**. APS coatings (Fig. 1a) usually exhibit a layered structure, with a swirl pattern and a large amount of voids and pores. The pores help to increase the insulating capacity of the oxide. VPS coatings (Fig. 1b) are also layered but are denser than APS coatings and the interface between the bond coat and the ceramic layer is generally more uniform than in air sprayed products. EBPVD coatings (Fig. 1c) have a dense columnar structure, which can accommodate the strains arising from differential thermal expansion between the metallic and ceramic layers.

Failure Modes of Thermal Barrier Coatings

The life of the overlay ceramic is limited by its susceptibility to thermal fatigue cracking, while the life of the bond coat is limited by its oxidation and corrosion behaviour. Hot corrosion of the ceramic overlay may also be life limiting in marine environments. The combined effects of stress, time at high temperatures and oxidizing environment are complex, causing changes in the microstructure of the coatings as well as the substrates. These changes eventually will lead to failure of the coatings. Transverse and longitudinal cracks form at the surface and inside the ceramic layer, due to thermally induced stresses. Oxidizing gases penetrate through the transverse cracks and oxidize the bond coat. The layer of Al_2O_3, which forms at the interface between the bond coat and the ceramic (and possibly between the bond coat and substrate), thickens during service. In this layer, oxidation products such as Cr_2O_3, NiO, HfO_2 and spinels ($NiO\text{-}Cr_2O_3\text{-}Al_2O_3$) are formed by loss of β-NiAl from the bond coat. In the case of EBPVD coatings, cracks form in this layer of oxides, causing the top ceramic coating to spall, whereas plasma sprayed coatings are known to fail above this oxide layer. The mechanisms of the reactions of the coatings with the environment in the engine and the ultimate coating failure are discussed in detail, elsewhere (**8-10**).

Evaluating Thermal Barrier Coatings

The effectiveness of a TBC coating is assessed from its ability to stay in place without spalling. The best way to assess coating durability is from actual engine tests. These, however, are expensive and time consuming. Alternatively, the performance of a coating can be evaluated in a burner rig, where engine operating conditions can be closely simulated. Engine manufacturers have used burner rig tests in the past to evaluate and compare the performance of coatings for screening purposes, prior to actual engine tests. In Canada, military operational groups have also relied on burner rig tests to assess the potential of emerging coatings for use in their engines, under various component retrofit programs. However, there is no standard procedure established for burner rig tests. Manufacturers and users adopt different cycling times and temperatures (heating times from a few minutes up to an hour, at temperatures from 1000°C to 1500°C, followed by cooling for a few minutes) tailored to suit their end use.

Objectives of the present study

At NRC, several studies have been performed using burner rig testing to compare TBC's produced by different techniques and different processing conditions, and to optimize some of the coatings for use in Canadian Forces engines. The objective of this paper is to discuss the testing procedures and methodologies employed in these studies with a view to evaluating the suitability and

practicality of burner rig testing as a laboratory ranking method for TBC's. The influence of key test parameters on modes and rates of damage accumulation is discussed. Ways to ensure that the modes known to be life limiting in engines are reproduced during rig testing are also addressed.

2. EXPERIMENTAL MATERIALS AND METHODS

2.1 Materials and Test Coupons

The TBC's investigated in this work included experimental coatings produced by EBPVD, APS and VPS, under three development programs, as well as TBC's produced by established techniques by commercial vendors. In the first series of tests, the performance of experimental EBPVD TBC's having compositionally and functionally graded interfaces between the metallic bond coat and the ceramic layer, was evaluated. These coatings were applied to nickel base superalloy pins, 0.25" diameter and 4" long, made from IN625 and a proprietary single crystal (7). In the second series of tests, zirconia and calcia based TBC's were plasma sprayed onto IN625 pins, 0.5" diameter and 5.5" long, using different conditions of particle velocities and temperatures, and studied to assess the effects of composition and processing conditions on product performance (**11,12**). In the third series of tests, the performances of a non-graded EBPVD TBC, TBC's with VPS bond coats and APS ceramic overlays and TBC's with VPS bond coats and VPS overlays, were also studied. These latter coatings were applied to the same pins as those used for the first series of tests.

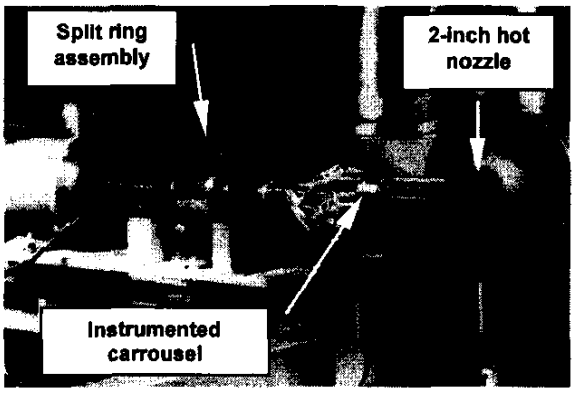

Figure 2 The IAR burner rig equipped with the 2-inch exhaust nozzle for testing ¼ inch diameter test pins. The slip rig assembly accommodates up to eight thermocouples for instrumentation of test pins

2.2 Testing and Evaluation

The coated pins were subjected to thermal cycling in a high velocity/atmospheric burner rig. The design of this rig is based on a dynamic combustor similar to that used in gas turbine engines (**13**). The mixing and flow in the combustor closely approximate conditions that exist within conventional combustors and the critical features of combustor chemistry are readily reproduced and controlled. This is particularly important when assessing the effects of gas/coating reactions on the durability of coatings (**14,15**). Fuel (JP-4), along with compressed air, is introduced through a pressure-atomizing nozzle into the primary section of the combustor, within which combustion occurs in a swirl stabilized recirculation zone. The expanding combustion gases are cooled by dilution within a secondary section, and are exhausted through a nozzle in front of which the test pieces are placed for exposure to high velocity hot gases. By independently adjusting the primary and secondary air flows, along with the fuel flow, it is possible to vary the gas velocity and gas temperature independently of each other. With a standard 2-inch axisymmetric circular exhaust nozzle, gas velocity can be varied from Mach 0.2 to Mach 0.8 and gas temperature from 540°C (1000°F) to 1650°C (3000°F). The latter is controlled by a programmable microprocessor and measured by a thermocouple located near the throat of the exhaust nozzle. Nozzles of different sizes can be used to vary the cross sectional geometry of the hot gas jet to accommodate different test piece geometries. In the present studies, the standard 2-inch diameter nozzle was used when testing the ¼" diameter pins and a 3-inch oversized nozzle was used for the ½" diameter pins. In both cases, the pins were positioned 1.5" away from the exhaust nozzle.

The rig in the standard 2-inch nozzle configuration is shown in **Figure 2**, with a set of uncoated ¼ inch diameter pins positioned in front of the exhaust nozzle. The test pins are mounted on a rotating carrousel, used to translate the pins back and forth between the hot gases and a jet of room temperature air from a 2-inch diameter pipe located beside the hot nozzle. In this way, the pins can be alternately heated and cooled, simulating thermal cycling in engines. Rotation of the pins, typically at 100 to 200 rpm, is used to promote gas mixing and ensure uniform exposure of the pins to the hot and the cold gases. An electrical slip ring assembly mounted on the drive shaft of the rotating carrousel can be used for instrumentation of 8 of the 12 test pins.

The rig in its 3-inch nozzle configuration is shown in **Figure 3**, with a set of coated ½ inch diameter pins positioned in front of the cooling nozzle. With the oversized carousel required to handle the ½ inch diameter pins, the larger exhaust nozzle was needed to achieve efficient heating of the pins. However, at equivalent air to fuel mass flow ratios, the gas velocities and the maximum heating rates and temperatures achievable with the 3-inch exhaust nozzle are not as large as those produced with the 2-inch nozzle, which has a bearing on the modes and rates of damage accumulation in coatings, as discussed below.

In the present studies, the temperatures at various locations at the surface and in the interior of the pins were monitored by thermocouples mounted flush with the surface and inside an axial blind hole. The changes in pin

surface temperature distribution, as a function of gas temperature and gas velocity and the changes in metal temperature at the core of the pins, as a function of number of thermal cycles, were established in this manner. For surface temperature measurements, holes drilled radially and along the axes of the pins were used as feedthroughs for the thermocouple leads, to avoid disturbing the heat transfer boundary layer around the pins. Several pins with one thermocouple each, and with thermocouple beads regularly spaced along the axes of the pins, were used for these measurements. A schematic cross section of the instrumented ½ inch diameter pins, where all the bead positions have been combined in a single drawing for simplicity, is shown in **Figure 4**. The surface temperature measurements were performed on bare pins.

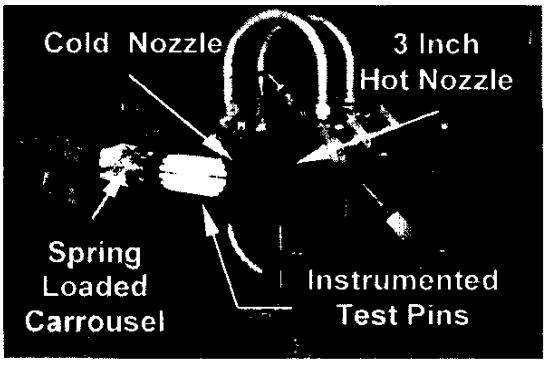

Figure 3 The IAR burner rig equipped with the 3-inch exhaust nozzle for testing ½ inch diameter test pins.

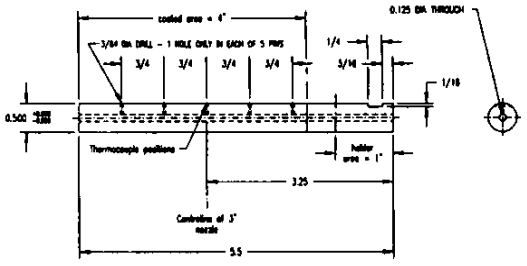

Figure 4 Schematic cross section of the instrumented ½ inch pins showing locations of surface thermocouples positioned at regular intervals along the pin length.

Internal temperatures were only measured in the case of the ½ inch diameter pins. The intent was to track the degradation in thermal protection efficiency of their TBC's as a function of number of thermal cycles, or test time, through measurements of drifts in heating and cooling rates during thermal cycling. To measure the internal metal temperatures, thermocouples (one per pin) were mounted with their beads pushed against the bottom of a blind hole drilled along the axes of the pins, using a spring-loaded mechanism. A schematic of the instrumented ½ inch diameter pin is shown in **Figure 5**, while a close-up view of the spring loaded mechanism is shown in **Figure 6**, with the test pins removed from the carrousel, but with the thermocouples still in place. The spring-loaded device ensured that the thermocouple beads were kept in contact with the bottom ends of the holes, irrespective of the degree of thermal expansion and contraction experienced by the pins during thermal cycling. The position of the bottom of the hole was chosen to correspond to the position within the hot gas jet known to experience the highest temperature, in order to record the maximum metal core temperatures.

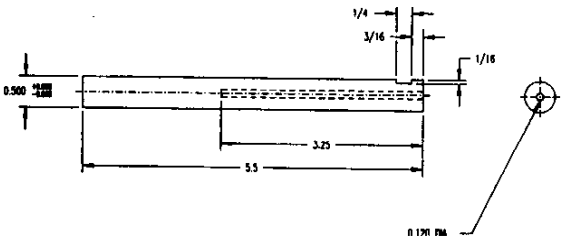

Figure 5 Schematic cross section of the instrumented ½ inch pins showing the axial blind hole within which thermocouples were held in positive contact with the bottom end of the holes to measure metal core temperatures of the pins reliably.

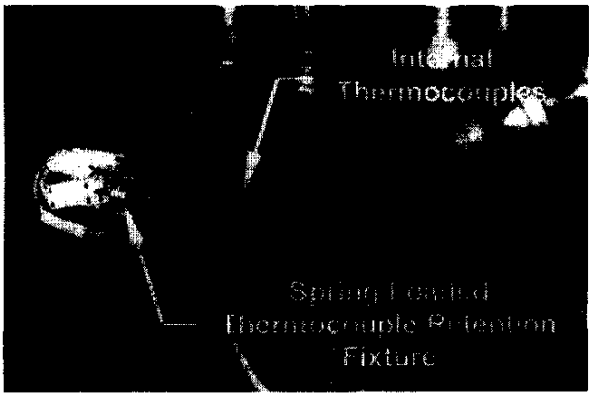

Figure 6 Close up view of the instrumented carrousel showing the spring loaded thermocouple retention fixture which ensured the thermocouple beads were kept in contact with the test pins (not shown) during thermal cycling.

Burner rig tests involved up to 2150 cycles of 4 minutes of heating in the high velocity hot gas jet followed by 2 minutes of forced air cooling. In some cases, the gas temperature was increased in a stepwise manner, from a minimum of 1300°C to a maximum of 1500°C, to increase the severity of the tests and ensure that failure of the coatings occurred before the end of the tests. The surface conditions of the pins and their weight to the nearest 0.5 mg were recorded before testing and after every 50 to 150 cycles. The weight changes provided a measure of the spalling resistance of the various TBC's to

the combined effects of thermal loads and hot gas erosion. Changes in the heating and cooling rates of the pins during thermal cycling were also extracted on-line from internal temperature measurements. Finally, the microstructures of the TBC's were compared before and after testing, and the extent of thermally induced microstructural changes, including phase transformation as revealed by x-ray diffraction, was assessed.

3. RESULTS AND DISCUSSION

3.1 Effects of Pin Size and Testing Conditions on Pin Temperatures

The variation of pin temperature during thermal cycling depends on the heat transferred between the pin and the hot and cold gas jets. This heat transfer is discussed in detail and modelled elsewhere, for the case of an airfoil-like test coupon (**16**). Considerable heat losses arise from radiation from the surface of the pins and by conduction towards their free ends and into the carrousel body. Consequently, the maximum temperatures reached by the pins are considerably lower than the maximum temperature of the impinging hot gases. A record of core temperatures over a complete thermal cycle (4 minutes of heating in Mach 0.22 1500°C gas, followed by 2 minutes of air cooling), for 12 coated ½ inch diameter pins, is shown in **Figure 7**. Pin temperatures are seen to rise rapidly at first until, after about two minutes, they stabilize. The maximum steady state temperature reached by the pins at the end of the heating cycle depends to some degree on the TBC and, on average, is about 350°C lower than the gas temperature.

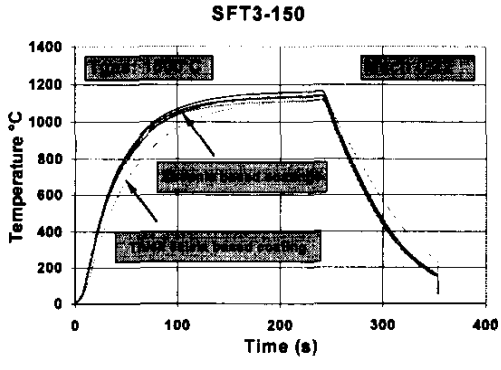

Figure 7 Typical thermal cycles experienced by ½ inch diameter pins as revealed by thermocouples inside axial blind holes in pins (see Figure 5).

The temperatures of a series of instrumented ½ inch diameter pins, as recorded by surface and internal thermocouples over parts of the heating portion of a thermal cycle, are shown in **Figure 8.** These data were obtained from 5 uncoated pins (T1 to T5), each equipped with a surface thermocouple, and 2 coated (Tc-Ca8 and Tc-Ca11) and one bare pin (Tc-bare), each equipped with one internal thermocouple. The core temperatures of the coated pins rise more slowly than those of the bare pins, due to the thermal insulating effect of the TBC's.

However, the coated pins reach higher steady state core temperatures than do the bare pins, as the rates of heat loss from the free ends of the coated pins are reduced relative to bare pins. Also, the internal temperatures of both bare and coated pins are higher than their surface temperatures. This difference increases with gas temperature and is higher in coated pins, as shown in **Table 1**.

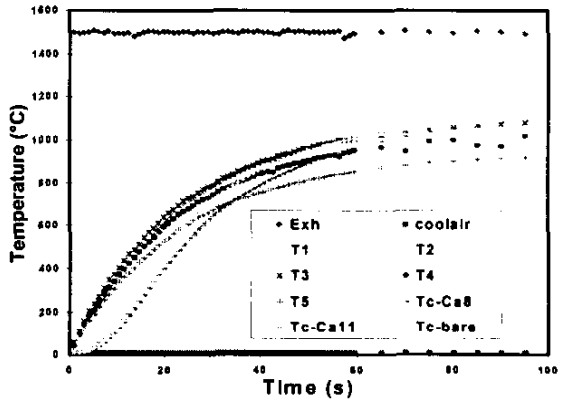

Figure 8. Surface and internal temperature histories revealed by instrumented test pins over parts of the heating portion of a thermal cycle involving 4 minutes of heating in Mach 0.22, 1500°C gas.

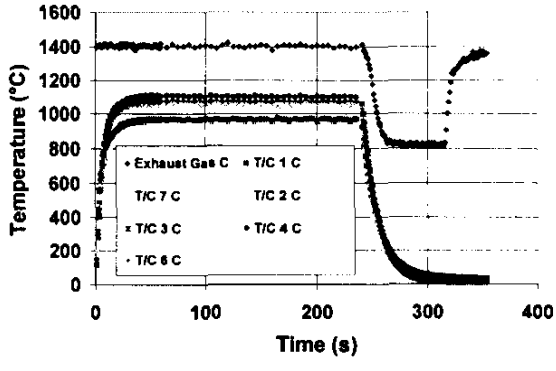

Figure 9 Surface temperature histories revealed by instrumented ¼ inch diameter pins over parts of the heating portion of a thermal cycle involving 4 minutes of heating in Mach 0.45 1400°C gas.

The heating and cooling rates for ¼ inch diameter pins during thermal cycling, and the maximum metal temperatures reached under steady state, were significantly higher than those observed on the ½ inch diameter pins, when tested at equivalent gas temperatures and mass flow rates of hot gas. For instance, at a gas temperature of 1400°C, with primary and secondary airflows adjusted to give a gas velocity of Mach 0.45, less than 20 seconds were needed for ¼ inch pins to reach their maximum steady state temperatures, as shown in

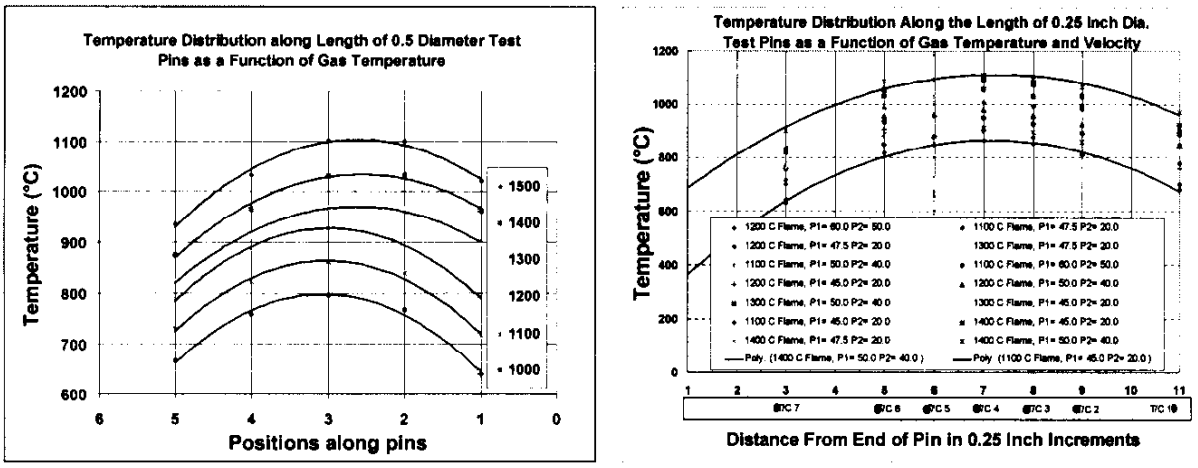

(a) (b)

Figure 10 Profiles of steady state pin (bare) surface temperatures for (a) ½ inch diameter pins, and (b) ¼ inch diameter pins, measured at different gas temperatures and gas velocities.

T_{gas} °C	Mach #	$T_{surface}$ (max)	T_{core} (bare)	T_{core} (coated)	ΔT (bare)	ΔT (coated)
1300	0.2	989	996	999	7	10
1400	0.22	1031	1048	1067	17	36
1500	0.22	1097	1122	1146	25	49

Table 1 Comparison of surface temperatures, axial temperatures and differences between the two for bare and coated ½ inch pins exposed to different gas temperatures and velocities.

Figure 9. This compares with more than 80 seconds for ½ inch pins, tested at a higher gas temperature of 1500°C, and the same primary and secondary air flows, **Figure 7**. When both types of pins were heated in a 1400°C gas jet, the maximum steady state temperature of ¼ inch diameter pins was of the order of 1100°C, whereas it was only 1040°C for ½ inch pins. This is shown in **Figure 10** which compares the surface temperatures of ¼ inch and ½ inch diameter bare pins measured at different axial positions along their lengths, over a broad range of gas temperatures and velocities (i.e. under different ratios of primary and secondary gas pressures). The differences in temperature at equivalent mass flow rates of hot gas can be ascribed to the higher velocities that were achieved with the smaller exhaust nozzle used with ¼ inch pins, typically Mach 0.45 for ¼ inch pins vs. Mach 0.22 for ½ inch pins. The temperature gradients along the length of both types of pin were, however, qualitatively similar.

These temperature gradients simulate those present on actual engine parts and can be adjusted to meet specific test requirements by varying pin length or pin position within the hot gas jet. At any given gas temperature and velocity, minimizing the length of the free end of a pin extending outside the gas jet, will increase maximum pin temperature, owing to decreased heat losses from the free end. Conversely, increasing the pin length will result in steeper longitudinal thermal gradients. These gradients can be used to advantage, and their shape optimized, to study the combined effects of thermal fatigue, gas erosion and hot corrosion of ceramic overlays and bond coats. With corrosive contaminants (sulfur in fuel plus atomized sea-salt solution in combustor air) added to the hot gas jet, those regions of the pins exposed to surface temperatures between 700°C to 900°C may suffer fluxing of the ceramic oxide overlays leading to breakdown of the TBC system. The contaminants may also penetrate along thermally induced cracks and attack the bond coat. These forms of hot corrosion could affect the regions of coated components where temperature drop below 900°C, in engines operating in marine environment. The burner rig test is an ideal tool to study the susceptibility of different TBC systems to this form of attack, and its interactions with other forms of thermally driven damage, should be investigated.

For durability assessment of coatings, it may be preferable to use ¼ inch rather than ½ inch diameter pins, because in addition to being more severely thermally shocked, the ¼ inch pins will accumulate more time at maximum temperature. Thus, over the same number of thermal cycles the bond coat on a ¼ inch pin will be oxidized more than on a ½ inch diameter pin. Accumulation of oxidation damage, can be life limiting in many applications (**8-10**) and is more easily simulated with ¼ inch diameter pins.

3.2 Damage Accumulation

The first sign of damage incurred by the TBC's during thermal cycling was in the form of a network of cracks developed over regions of both the ¼ and ½ inch pins

exposed to the hot gases. The cracked surface of an EBPVD coating on a ¼ inch pin, after some thermal cycling had been applied, is shown in **Figure 11**.

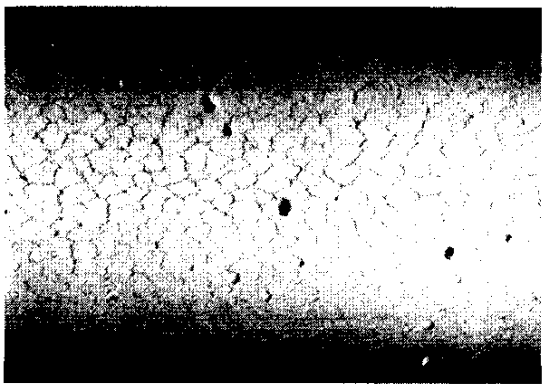

Figure 11 Network of surface cracks formed on EBPVD TBC's soon after initiation of thermal cycling in burner rig.

The cracks in this instance penetrate right down to the bond coat, as revealed in **Figure 12**. A thin oxide layer has formed at the ceramic bond coat interface, where delamination occurred. Networks of cracks were also observed in plasma sprayed coatings. The density of cracks and their morphology depended on processing conditions and the degree of cracking was usually more severe in thicker coatings. Cracks were present even in as-deposited APS coatings, when the ceramic layer was thick (300-400 μm).

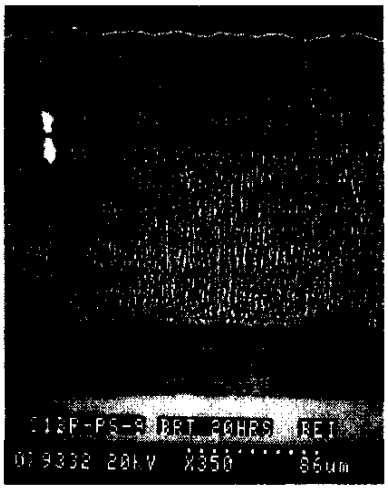

Figure 12 Metallographic cross-section through EBPVD TBC showing transverse crack through coating penetrating all the way down to the bond coat.

Ablation from the surface of the TBC's due to erosive action of the high velocity hot gases was also observed on all the coatings examined. In the latter stages of the tests, most of the TBC's experienced spalling, or delamination, of their ceramic topcoats. The number of cycles to spalling initiation varied with the deposition method, and even more significantly, with processing conditions for each of the deposition methods. Some coatings from all four forms of TBC's investigated (EBPVD, APS, VPS/APS and VPS) were found to survive temperatures up to 1500°C for several hundred cycles, without spalling. A series of APS TBC's, after rig testing are shown in **Figure 13**. The 1.2 mm thick calcia based coating, (pin (a) in Figure 13), shows no evidence of spalling, whereas the zirconia based TBC's (all about 300 μm thick, pins (b) to (f),) exhibit varying degrees of delamination.

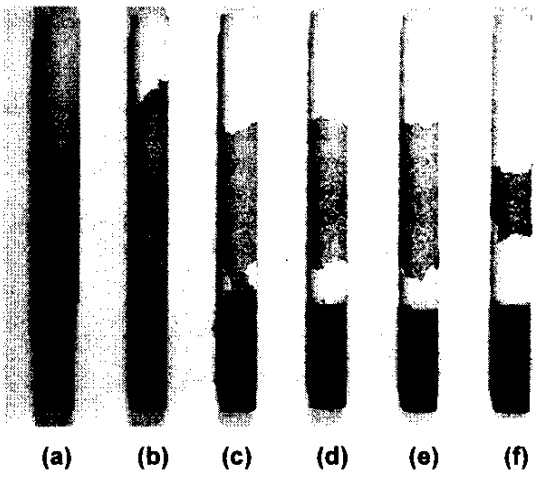

Figure 13 Conditions of a series of APS coated ½ inch pins at the end of burner rig testing, involving 2150 cycles at temperatures up to 1500°C; (a) 1.2 mm thick calcia-based TBC; (b) to (f) zirconia-based TBC's applied under different processing conditions.

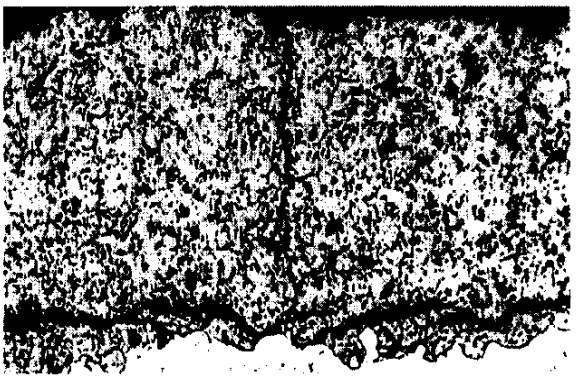

Figure 14. Micrographs illustrating onset of failure mechanism in zirconia based APS TBC, by cracking above the interface with the bond coat.

A thin layer of ceramic coat remained attached to the surface of the hottest sections of the zirconia pins. This is due to spalling occurring in these APS coatings by propagation and linking of cracks, about 30 μm above the

surface of the bond coat, as shown in **Figure 14**. The vertical cracks may relieve the stresses at the interface, thereby reducing the driving force for delamination. One of the pins, (b) in **Figure 13**, shows evidence of bond coat oxidation, where the ceramic topcoat has been entirely eroded away by the hot gases. These observations are generally consistent with expected modes of failure for APS coatings (**8-10**).

3.3 Damage Monitoring and Quantification

Weight Change Measurements
Changes in the weight of some coated ½ inch pins, measured over 1150 thermal cycles, are presented in **Figure 15**. The weight losses observed for all the TBC's are due to gas-induced ablation and spalling of the topcoats, during the test. The thick APS calcia-based coating appeared to have incurred the least damage in this test, while the performance of APS zirconia-based coatings varied greatly with processing conditions. The relationships between processing conditions, microstructures and properties of APS coatings are being investigated at NRC and the results will be published elsewhere (**11,12**).

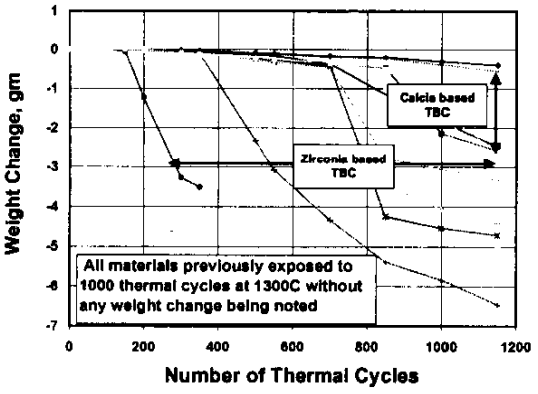

Figure 15 Changes in mass of a series of APS coated ½ inch pins as a function of number of thermal cycles over a test 100 cycles at 1350°C followed by 1050 cycles at 1500°C.

Changes in the weight of some coated ¼ inch pins processed by EBPVD, VPS (bond)/APS (ceramic) and VPS are presented in **Figure 16**. All coatings experienced weight gains at the onset of testing. This is from oxidation of the bond coats and, possibly absorption of oxygen by the substoichiometric zirconia of the VPS coatings. Because the ¼ inch pins spent more time at the maximum gas temperature, as compared to ½ inch pins, (see **Figures 7 and 9** for comparison), there was more time available for their metallic bond coats to oxidize, in the course of the test. This was followed by weight loss from ablation and spalling of the ceramic topcoats, until the temperature was raised from 1200°C to 1300°C and higher, beyond which the weights increased again. These trends are due to the rate of bond coat oxidation increasing with temperature.

The data shown in **Figure 16** also reveal that processing conditions during deposition can be adjusted to achieve improved performance with VPS coatings. The optimized VPS coating showed minimum weight changes for more than 1000 cycles at gas temperatures up to 1400°C, indicative of good resistance to ablation and spalling. However, it spalled off rapidly after the temperature was raised to 1500°C, as did the APS coatings.

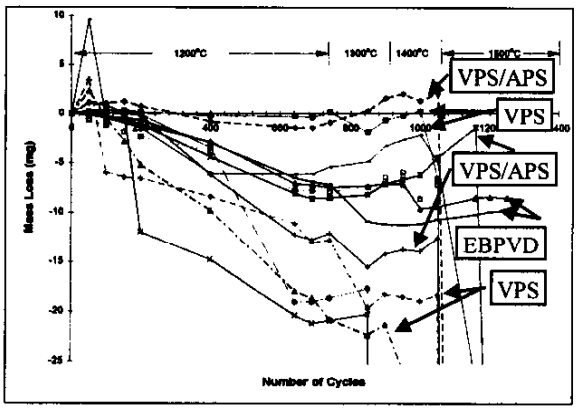

Figure 16 Changes in the mass of a series of EBPVD, APS and VPS coatings applied to ¼ inch pins as a function of number of rig thermal cycles. The thermal cycling schedule is shown in the figure

Only the EBPVD coating survived the entire duration of the thermal cycling at 1500°C, because of the higher strain tolerance of its columnar microstructure. The apparent shortcoming of APS coatings should be viewed with caution, however, because the test conditions were not entirely representative of service conditions. The stresses within the coatings, caused by the difference in thermal expansion between the coatings and substrates were much larger in pins than those expected to prevail in actual service parts, which are cooled by internal air flow. The internal metal temperatures of the uncooled pins were actually greater than the surface temperatures, by up to 50°C at the centre of the pins under steady state conditions, as seen from **Table 1**. Under these conditions, the ceramic/metallic bond coat interface would be subjected to very large shear stresses conducive to accelerated spalling, as observed experimentally Thus the coatings on pins may have faced conditions that were too severe, possibly representing an extreme limiting case for plasma sprayed coatings. Using internally cooled pins and ensuring that adequate time is spent at maximum temperature during thermal cycling, to promote bond coat oxidation as experienced in service, would provide a more realistic testing environment and possibly different TBC ranking. Work is underway at IAR to address this issue.

Heating Rates Measurements

The maximum heating rates experienced by coated ½ pins, as measured by thermocouples located inside the pin's axial blind holes, are plotted in **Figure 17** as a function of the number of thermal cycles. Each data point in **Figure 17** corresponds to the maximum slope of the rising portions of the temperature/time curves obtained for each of the thermal cycles, examples of which are shown in **Figures 7 and 8.** There are several features in **Figure 17** that warrant comment. Firstly, the discontinuities in the data arise from interruptions in the test sequence required to weigh the pins, following blocks of 5, 50 or 150 thermal cycles. The initial sharp drop in heating rates at the onset of each block is due to the pins being at room temperature at the onset of the first cycle in a block, and at greater than room temperature for subsequent cycles, because the pins do not cool down fully to room temperature at the end of a cycle (see Figure 7).

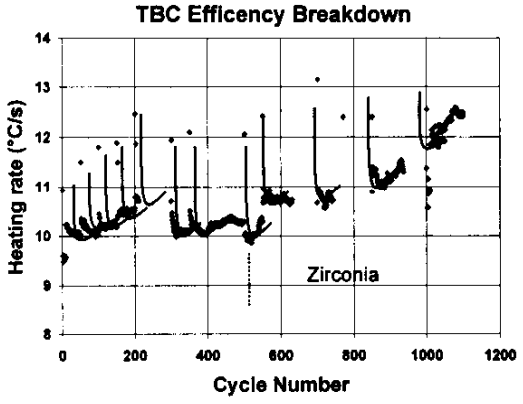

Figure 17 Changes in heating rates of a ½ pin coated with zirconia as function of number of thermal cycles applied to the pin, showing change in heat transfer characteristics of coated system.

As the temperature at the start of a cycle increases, the apparent heating rate inside the pin decreases. It takes several cycles for heating rates to become stable because of the complex heat transfer transients affecting the pins and their supporting carrousel. Secondly, the general upward trend in the data, observed within each block and from block to block across the plot, may be viewed as an indication of the breakdown in thermal protection efficiency of the TBC system. As the coating ablates, or spalls off the test pin, the internal heating rates increase, as expected, because heat is transferred more quickly into the pins. Thirdly, there appears to be a threshold number of applied thermal cycles beyond which the increase in heating rate accelerates sharply. This threshold is of the order of 500 cycles, and corresponds to the point beyond which significant weight loss was recorded for this coating, as shown in **Figure 15.** Thus, monitoring the internal temperatures of coated pins could be used as an alternative method for the quantification of damage accumulation in TBC's. However, further work is needed to develop this technique. The type K thermocouples that were used in the present experiments tended to oxidize and fail by thermal fatigue. Type S thermocouples should perform better in this application and ought to be tested. Also, the measurements should be made on pins that are internally cooled to better simulate the thermal gradients and levels of thermally induced stresses experienced by TBC's applied to internally cooled components.

CONCLUSIONS

This work has shown that the modes and rates of degradation of TBC's during burner rig testing of coated solid round pins are influenced by many test parameters, besides being influenced by differences in deposition method and processing conditions.

Pins, ¼ inch in diameter, heat up and cool down much faster than ½ inch pins. They also reach a higher temperature and spend more time at maximum temperature over the duration of a thermal cycle. Thus, coatings applied to ¼ inch pins will be subjected to higher transient and steady state stresses, and their bond coat will oxidize more in the course of a test, as compared to ½ inch pins.

Over the steady state portion of a thermal cycle, the internal temperature of a solid pin is higher than its surface temperature. This difference is larger in a TBC coated pin than in a bare pin. High internal temperatures in coated pins cause high shear stresses near the interface between the ceramic and metallic layers of the TBC, owing to differential thermal expansion between the two media, thereby promoting delamination near this interface. Because of their highly strain tolerant columnar microstructure, EBPVD coatings generally fared better than thermally sprayed coatings under such testing conditions. Using internally cooled pins, to better simulate service conditions, would reduce the magnitude of these stresses and provide a more realistic laboratory ranking of TBC coatings.

The performance of each type of TBC examined, is a strong function of processing conditions. Analysis of damage modes arising from thermal cycling in a rig confirms that plasma sprayed coatings spall by cracking of the ceramic overlay, above the interface with the bond coat, and in the case of EBPVD coatings, by cracking within the oxide layer that builds up at the surface of the bond coat. The failure modes differ because of differences in the degree of strain tolerance of the two types of coatings.

ACKNOWLEDGEMENTS

This work was performed at IAR and IMI under projects involving collaboration with a number of companies (Cametoid Advanced Technologies Inc., Pyrogenesis Inc., Orenda Aerospace Corporation, SURFTEC Industrial Consortium), with financial support from the Chief Research and Development of the Department of National Defense. Special thanks are due to Mr. Ray Dainty of IAR, for his support in SEM analysis.

REFERENCES

1. R.A. Miller, "Thermal Barrier Coatings for Aircraft Engines", Proc. Thermal Barrier Coating Workshop, NASA Lewis Research Center, Cleveland, Ohio, March 1995, NASA Conf. Pub. 3312, 1995, pp17-34.

2. P.E. Hodge, S. Stecura, M.A. Gedwill, I. Zaplatynski and S.R. Levine, "Thermal Barrier Coatings", J. Materials for Energy Systems, Vol. 1, 1980, pp. 47-58.

3. H. Herman and C.C. Berndt, "Plasma Spray Processing of TBC's", Proc. Thermal Barrier Coating Workshop, NASA Lewis Research Center, Cleveland, Ohio, March 1995, NASA Conf. Pub. 3312, 1995, pp. 127-134.

4. D.V. Rigney, R. Viguie and D.J. Wortman, "PVD Thermal Barrier Coating Applications and Process Developments for Aircraft Engines", Proc. Thermal Barrier Coating Workshop, NASA Lewis Research Center, Cleveland, Ohio, March 1995, NASA Conf. Pub. 3312, 1995, pp. 135-149.

5. S. Durham, S. Manning Maier, D.K. Gupta and K.D. Schefler, "Ceramic Thermal Barrier Coatings", in Advances in High Temperature Structural Materials and Protective Coatings, Eds. A.K. Koul et al, Pub. NRC, Canada, Ottawa, 1994, pp.226-236

6. Anonymous, "Vacuum plasma spray coating protects turbine blades", a note in Advanced Materials and Processes, March 1997, p. 12.

7. F. Jamarani, M. Korotkin, R.V. Lang, M.F. Ouelette, K.L. Yan, R.W. Bertram and V.R. Parameswaran, "Compositionally Graded TBC for High Temperature Aero Gas Turbine Components", Surface and Coatings Technology, 54/55, 1992, pp. 58-63.

8. M. Gell, "Application Opportunities for Nanostructured Materials and Coatings", Materials Science and Engineering, Vol. A204, 1995, pp. 246-251.

9. J. H. Wood and E.H. Goldman. "Protective Coatings" in *Superalloys-II*, Eds. C.T. Sims et al, Pub. John Wiley and Sons, 1987, pp. 359-384.

10. W.J. Brindley and R.A. Miller, "Thermal Barrier Coatings Evaluation Needs", Pres. at Conf. on *NDE of Modern Ceramics*, Columbus, OH, 9-12 July 1990, Am. Cer. Soc. & Am. Soc. for NDT, 1990, pp70-76 (NASA Report, NASA-TM-103708, 1990).

11. M. Prystay, P. Gougeon, C. Moreau, J-P. Immarigeon and V.R. Parameswaran, "Microstructure and Burner Rig Evaluation of Calcia Silica Thermal Barrier Coatings", Proceedings ITSC 98, Nice, France, May 1998.

12. P. Gougeon, M. Prystay, C. Moreau, J-P. Immarigeon and V.R. Parameswaran, "Influence of Plasma Spraying Conditions on In-Flight Characteristics of Zirconia Hollow Sphere Particles and Properties of Resulting TBC's", Proceedings ITSC 98, Nice, France, May 1998.

13. R.R. Dills and F.S. Follansbee, Corrosion, NACE, 1977, 33(11), 385.

14. A.K. Gupta, T. Terada, P.C. Patnaik and J-P. Immarigeon, "Evaluation of High Temperature Protective Coatings for Gas Turbine Engines Under Simulated Service Conditions", Proc. AGARD-NATO Conf. on High Temperature Surface Interactions, Ottawa, May 1989, AGARD-CP-461, 1989, pp. 14-1/14-31.

15. A.K. Gupta, J-P. Immarigeon and P. C. Patnaik, "A Review of Factors Controlling the Gas Turbine Hot Section Environment and their Influence on Hot Salt Corrosion Test Methods", High Temp. Technology, Vol. 7, No. 4, November 1989, pp. 173-186.

16. S. Gendron, N.J. Marchand, C. Korn, J-P. Immarigeon and J.J. Kacpryzynski, "An Experimental Investigation of Convective Heat Transfer at the Leading Edge of a Turbine Airfoil", Int. Gas Turbine and Aeroengine Congress and Expositttion, Cologne, Germany, June 1992, Publication ASME 92-GT-248, 1992